NUMERICAL EXPERIMENTS WITH 2D AND 3D TRANSONIC FLOWS

Trefilík, Jiří
Faculty of Mechanical Engineering, Czech Technical University

Huml, Jaroslav
Faculty of Mechanical Engineering, Czech Technical University

Kozel, Karel
Department of Applied Mathematics, Faculty of Mechanical Engineering, Czech Teclmical University

Příhoda, Jaromír
Institute of Thermomechanics, Czech Academy of Science

出版情報：COE Lecture Note. 36, pp.94-107, 2012-01-27. 九州大学マス・フォア・インダストリ研究所
バージョン：
権利関係：

Proceedings of the Czech–Japanese Seminar in Applied Mathematics 2010
Czech Technical University in Prague, August 30 - September 4, 2010
pp. 94–107

NUMERICAL EXPERIMENTS WITH 2D AND 3D TRANSONIC FLOWS

JIŘÍ TREFILÍK[1], JAROSLAV HUML[1], KAREL KOZEL[2] AND JAROMÍR PŘÍHODA[2]

Abstract. This work deals with the development of numerical methods for simulation of transonic flows of an inviscid and a viscous (turbulent) compressible fluid in a two- and three-dimensional channel and in the DCA 8% cascade. Results of numerical experiments modelling the inviscid and viscous flows at the different inlet Mach numbers are compared and discussed. The numerical solution was obtained by the finite volume method using Lax-Wendroff scheme (MacCormack's and Richtmyer's form) and the multistage Runge-Kutta method on structured non-orthogonal grids. Jameson's artificial dissipation was added to increase of the numerical stability. In the case of inviscid flows two different inlet boundary conditions are considered. For turbulence modelling algebraic Baldwin-Lomax model and two equations $k-\omega$ model were applied.

Key words. inviscid flow, viscous flow, turbulence modelling, finite volume method

AMS subject classifications. 65M06, 65M08

1. Mathematical models.

1.1. Navier-Stokes equations. The two-dimensional laminar flow of a viscous compressible liquid is described by the system of Navier-Stokes equations

$$W_t + F_x + G_y = R_x + S_y \tag{1.1}$$

where

$$W = \begin{pmatrix} \rho \\ \rho u \\ \rho v \\ e \end{pmatrix},\ F = \begin{pmatrix} \rho u \\ \rho u^2 + p \\ \rho uv \\ (e+p)u \end{pmatrix},\ G = \begin{pmatrix} \rho v \\ \rho uv \\ \rho v^2 + p \\ (e+p)v \end{pmatrix} \tag{1.2}$$

and

$$R = \begin{pmatrix} 0 \\ \tau_{xx} \\ \tau_{xy} \\ u\tau_{xx} + v\tau_{xy} + \lambda T_x \end{pmatrix},\ S = \begin{pmatrix} 0 \\ \tau_{xy} \\ \tau_{yy} \\ u\tau_{xy} + v\tau_{yy} + \lambda T_y \end{pmatrix} \tag{1.3}$$

with shear stresses given for the laminar flow by equations

$$\tau_{xx} = \frac{2}{3}\eta(2u_x - v_y),\ \tau_{xy} = \eta(u_y + v_x),\ \tau_{yy} = \frac{2}{3}\eta(-u_x + 2v_y). \tag{1.4}$$

This system is enclosed by the equation of state

$$p = (\kappa - 1)\left[e - \frac{1}{2}\rho(u^2 + v^2)\right]. \tag{1.5}$$

[1]Faculty of Mechanical Engineering, Czech Technical University in Prague, Prague CZ-121 35, Czech Republic.
[2]Institute of Thermomechanics, Czech Academy of Science, Prague CZ-182 00, Czech Republic.

In the above given equations, ρ denotes density, u, v are components of velocity in the direction of axis x, y, p is pressure, e is total energy per a unit volume, T is temperature, η is dynamical viscosity and λ is thermal conductivity coefficient. The parameter $\kappa = 1.4$ is the adiabatic exponent.

1.2. Reynolds averaged Navier-Stokes equations. For the modelling of a turbulent flow, the system of RANS (Reynolds Averaged Navier-Stokes) equations enclosed by a turbulence model is used. Two different turbulence models with the turbulent viscosity were tested, one algebraic, Baldwin-Lomax and the two-equation $k - \omega$ model according to Wilcox. The system of averaged Navier-Stokes equations is formally the same as (1.1), but this time the flow parameters represent only mean values in the Favre sense, see [3]. The shear stresses are given for the turbulent flows by equations

$$\begin{aligned} \tau_{xx} &= \frac{2}{3}(\eta + \eta_t)(2u_x - v_y) \\ \tau_{xy} &= (\eta + \eta_t)(u_y + v_x) \\ \tau_{yy} &= \frac{2}{3}(\eta + \eta_t)(-u_x + 2v_y) \end{aligned} \tag{1.6}$$

where η_t denotes the turbulent dynamic viscosity according to the Boussinesq hypothesis. The Reynolds number is defined by $Re = \frac{u_\infty L}{\eta_\infty}$ and the Mach number by $M = \sqrt{\frac{q}{a}}$ where $q = \sqrt{(u^2 + v^2)}$ and a is the local speed of sound.

All the computations were carried out using dimensionless variables with reference variables given by inflow values. The reference length L is given by the width of the computational domain.

2. Turbulence models.

2.1. Baldwin-Lomax model. Algebraic models are based on the model proposed for the boundary-layer flows by Cebeci and Smith. Baldwin-Lomax model is its modification applicable for general turbulent shear flows. The boundary layer is divided into two regions. In the inner (nearest to the wall) part, the turbulent viscosity is given by

$$\eta_t = \rho F_D^2 \kappa^2 y^2 |\Omega| \tag{2.1}$$

where Ω is the vorticity, which is in the 2D flow determined by

$$\Omega = \frac{\partial u}{\partial y} - \frac{\partial v}{\partial x}. \tag{2.2}$$

and

$$F_D = 1 - exp\left(-\frac{y^+}{A^+}\right). \tag{2.3}$$

$y^+ = \frac{u_* y}{\nu}$ denotes dimensionless distance from the wall, $\nu = \frac{\mu}{\rho}$ is kinematic viscosity, $u_* = \sqrt{\left(\frac{\tau_w}{\rho}\right)}$ is so called friction velocity and $\tau_w = \mu \left(\frac{\partial u}{\partial y}\right)_{y=0}$.

The turbulent viscosity in the outer region is given by

$$\eta_{to} = \alpha\rho C_{cp} F_w F_k \tag{2.4}$$

where C_{cp} is a constant. Function F_w is determined by the relation

$$F_w = y_{max} F_{max} \tag{2.5}$$

for F_w being the maximum of the function

$$F = y F_D |\Omega| \tag{2.6}$$

and y_{max} the distance from the wall in which $F(y_{max}) = F_{max}$ holds and

$$F_k = \left[1 + 5.5\left(C_{KL}\frac{y}{y_{max}}\right)^6\right]^{-1}. \tag{2.7}$$

The Baldwin-Lomax model (1978) contains following values of the constants: $\kappa = 0.4$, $A^+ = 26$, $\alpha = 0.0168$, $C_{cp} = 1.6$, $C_{KL} = 0.3$.

2.2. $k - \omega$ **model.** Two-equation models are based on transport equations for two characteristic scales of turbulent motion, mostly for the turbulent energy k and dissipation rate ϵ, often used in the form of specific dissipation rate $\omega = \epsilon/k$. These characteristics are computed from transport equations. Turbulent viscosity is defined as

$$\eta_t = \rho\frac{k}{\omega}. \tag{2.8}$$

The standard Wilcox $k - \omega$ model is formed by the equations

$$\frac{\partial}{\partial t}(\rho k) + \frac{\partial}{\partial x_j}(\rho u_j k) = P_k + \frac{\partial}{\partial x_j}\left[(\eta + \sigma^*\eta_t)\frac{\partial k}{\partial x_j}\right] - \beta^*\rho k\omega \tag{2.9}$$

$$\frac{\partial}{\partial t}(\rho\omega) + \frac{\partial}{\partial x_j}(\rho u_j \omega) = \gamma\frac{\omega}{k}P_k + \frac{\partial}{\partial x_j}\left[(\eta + \sigma\eta_t)\frac{\partial \omega}{\partial x_j}\right] - \beta\rho\omega^2 \tag{2.10}$$

where $P_k = \tau_{ij}\partial u_i/\partial x_j$ represents the production of turbulent energy. Model coefficients are given by values: $\alpha = 5/9$, $\beta = 3/40$, $\beta^* = 9/100$, $\sigma = 1/2$ and $\sigma^* = 1/2$, $i, j \in \{1, 2\}$.

3. Numerical methods. For the modelling of the flow cases three finite volume method numerical schemes were used on non-orthogonal structured grids of quadrilateral and hexahedral cells $D_{ij(k)}$.

- the Lax-Wendroff scheme – MacCormack form (**MC**)

predictor step

$$W_{i,j}^{n+1/2} = W_{i,j}^n - \frac{\Delta t}{\mu_{i,j}}\sum_{k=1}^{4}\left[\left(\tilde{F}_k^n - \frac{1}{Re}R_k^n\right)\Delta y_k - \left(\tilde{G}_k^n - \frac{1}{Re}S_k^n\right)\Delta x_k\right] \tag{3.1}$$

corrector step

$$W_{i,j}^{n+1} = \frac{1}{2}(W_{i,j}^n + W_{i,j}^{n+1/2}) - \frac{\Delta t}{2\mu_{i,j}}\sum_{k=1}^{4}\left[\left(\tilde{F}_k^{n+1/2} - \frac{1}{Re}R_k^{n+1/2}\right)\Delta y_k + \right.$$
$$\left. - \left(\tilde{G}_k^{n+1/2} - \frac{1}{Re}S_k^{n+1/2}\right)\Delta x_k\right] + AD(W_{i,j}^n) \tag{3.2}$$

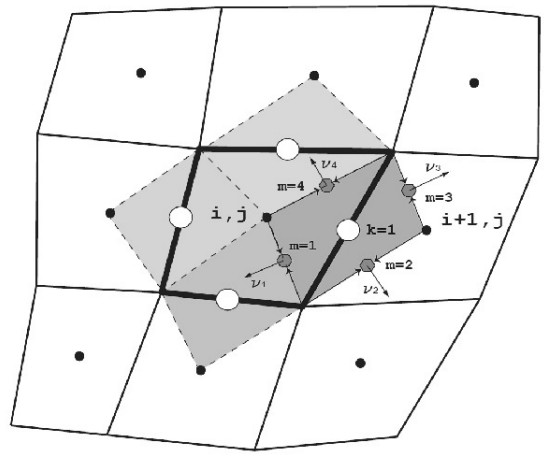

FIG. 3.1. *Evaluation of a derivative in the center of an edge*

The Mac Cormack scheme in the cell centered form was applied in solving the system of RANS equations. Convective terms F, G are considered in predictor step in forward form and in the corrector step in upwind form of the first order of accuracy, dissipative terms in central form of the second order of accuracy. To indicate this we denote their numerical approximation as $\tilde{F}$, $\tilde{G}$.

- the Lax-Wendroff scheme – Richtmyer form (**Ri**)

predictor step

$$W_{i,j}^{n+1/2} = W_{i,j}^{n} - \frac{\Delta t}{2\mu_{i,j}} \sum_{k=1}^{4} \left(\tilde{F}_k^n \Delta y_k - \tilde{G}_k^n \Delta x_k \right) \tag{3.3}$$

corrector step

$$W_{i,j}^{n+1} = W_{i,j}^{n} - \frac{\Delta t}{\mu_{i,j}} \sum_{k=1}^{4} \left(\tilde{F}_k^{n+1/2} \Delta y_k - \tilde{G}_k^{n+1/2} \Delta x_k \right) + AD(W_{i,j}^n) \tag{3.4}$$

- the multistage Runge-Kutta method (**RK**)

$$ResW_{i,j,k}^{(r)} = \frac{1}{\mu_{i,j,k}} \sum_{l=1}^{6} \left(\tilde{F}, \tilde{G}, \tilde{H} \right)_{i,j,k,l} \cdot \vec{n}_{i,j,k,l}^{0} \Delta S_{i,j,k,l} \tag{3.5}$$

$$\begin{aligned} W_{i,j,k}^{(0)} &= W_{i,j,k}^{n} \\ W_{i,j,k}^{r+1} &= W_{i,j,k}^{(0)} - \alpha_r \Delta t ResW_{i,j,k}^{(r)} + AD(W_{i,j,k}^n), \ r = 0,1,2 \\ W_{i,j,k}^{n+1} &= W_{i,j,k}^{(3)} \\ \alpha_{0,1} &= 0.5, \ \alpha_2 = 1 \end{aligned} \tag{3.6}$$

In all the previous cases the value $\mu_{ij(k)}$ represents the surface (volume) of the cell. Figure 3.1 shows evaluation of derivatives on edges of cells: We imagine a virtual cell as shown in the picture. We know the values in the centers of the cells and we define the other two as a mean value of its surrounding cells. From that we extrapolate to its edges and then we apply Green's formula.

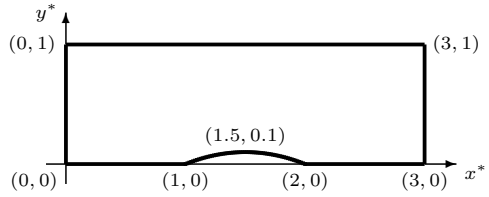

FIG. 4.1. *test case GAMM*

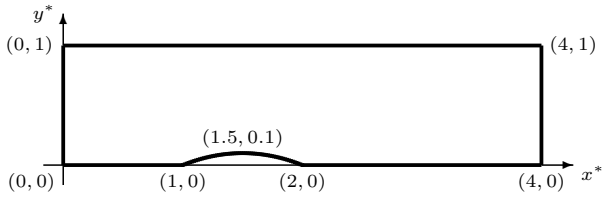

FIG. 4.2. *test case* LONG

Each scheme was extended to include Jameson's artificial dissipation because of the stability of the method

$$
\begin{aligned}
AD(W^n_{i,j,k}) = {} & C_1\psi_1(W^n_{i-1,j,k} - 2W^n_{i,j,k} + W^n_{i+1,j,k}) \\
& + C_2\psi_2(W^n_{i,j-1,k} - 2W^n_{i,j,k} + W^n_{i,j+1,k}) \\
& + C_3\psi_3(W^n_{i,j,k-1} - 2W^n_{i,j,k} + W^n_{i,j,k+1})
\end{aligned} \tag{3.7}
$$

where

$$
\begin{aligned}
\psi_1 &= \frac{\left|p^n_{i-1,j,k} - 2p^n_{i,j,k} + p^n_{i+1,j,k}\right|}{\left|p^n_{i-1,j,k}\right| + \left|p^n_{i,j,k}\right| + \left|p^n_{i+1,j,k}\right|}, \\
\psi_2 &= \frac{\left|p^n_{i,j-1,k} - 2p^n_{i,j,k} + p^n_{i,j+1,k}\right|}{\left|p^n_{i,j-1,k}\right| + \left|p^n_{i,j,k}\right| + \left|p^n_{i,j+1,k}\right|}, \\
\psi_3 &= \frac{\left|p^n_{i,j,k-1} - 2p^n_{i,j,k} + p^n_{i,j,k+1}\right|}{\left|p^n_{i,j,k-1}\right| + \left|p^n_{i,j,k}\right| + \left|p^n_{i,j,k+1}\right|}.
\end{aligned} \tag{3.8}
$$

The convergence to the steady state is followed by log L_2 residual defined by

$$
ResW^n = \sqrt{\frac{1}{M}\sum_k \left(\frac{W^{n+1}_k - W^n_k}{\Delta t}\right)} \tag{3.9}
$$

where M is a number of all cells in the computational domain.

4. Formulation of the problems. There were 4 types of computational domains, we denote them as GAMM, DCA, LONG (a 2D extended modification of GAMM channel that represent the lower half of the computational domain and where the upper part of the boundary represents a symmetry axis) and SWEPT WING (a 3D modification of GAMM where a middle part of the lower wall represents the upper half of a swept wing). Their outlines are presented in the figures Fig. 4.1 – 4.4.

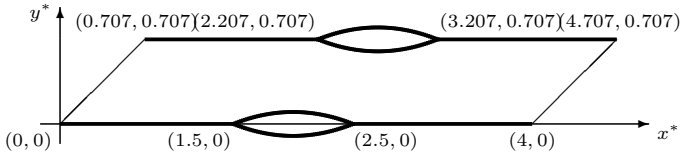

FIG. 4.3. *test case DCA*

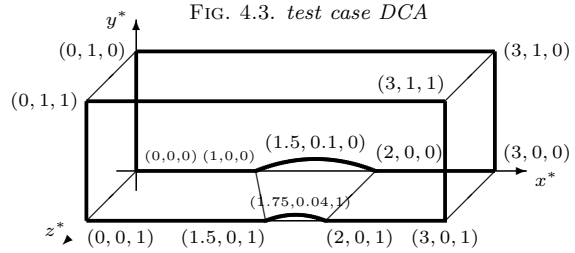

FIG. 4.4. *test case* SWEPT WING

4.1. Boundary conditions. On the **inlet** we considered two types of inlet boundary conditions (IBC):

$\mathcal{A}$ $\rho_1 = 1,\ u_1 = M_1 \cos\alpha_1,\ v_1 = M_1 \sin\alpha_1,\ w_1 = 0,\ p_1$ was extrapolated from the flow field and e_1 was calculated using the equation of state.

$\mathcal{B}$ $\rho_1 = 1,\ u_1 = M_1 \cos\alpha_1,\ v_1 = M_1 \sin\alpha_1,\ w_1 = 0,\ p_1 = 1/\kappa = 0.714$ and e_1 was calculated using the equation of state.

Inlet boundary conditions IBC $\mathcal{A}$ were used for inviscid compressible flows in GAMM, DCA and SWEPT WING; IBC $\mathcal{B}$ were used for inviscid compressible flows in GAMM, DCA and for viscous (turbulent) flows in LONG. The angle of attack α_1 could be nonzero just in the case of flows through DCA cascade.

On the **outlet** we prescribed only pressure $p_2 = p_1$ and the rest was extrapolated from the flow field.

Further on there are three other types of boundary conditions: solid wall, symmetry axis and periodicity. These conditions are implemented by using virtual cells. Such cells adjoin from outside on the boundary cells and we prescribe values of unknowns inside of them to obtain the desired effect.

Solid wall (an inviscid flow): velocity components prescribed so that the sum of velocity vectors equals to zero in its tangential component. **Solid wall (a viscous flow)**: velocity components were prescribed so that the sum of velocity vectors equals zero. In both cases the rest of unknowns is the same in both the virtual and the boundary cell.

Symmetry axis: this condition was realized by the same way as the wall condition for an inviscid flow.

Periodicity condition: taking two corresponding segments of boundary we prescribe into virtual cells of the first segment the values of unknowns contained in the boundary cells of the second and vice-versa.

Initial conditions were prescribed to comply with the inlet conditions.

5. Numerical results. First results of the inviscid compressible flow in the GAMM are presented. These results that were obtained by Lax-Wendroff schemes – MacCormack form (**MC**, see Fig. 6.1, 6.2) and Richtmyer form (**Ri**, Fig. 6.3) – and by the multistage Runge-Kutta method (**RK**, Fig. 6.5) were compared both each others (two types of inlet boundary conditions – IBC $\mathcal{A}$, $\mathcal{B}$).

The second test case of inviscid compressible flows was a flow through the DCA

8% cascade whose numerical solution was obtained by **MC** (Fig. 6.6) and **RK** scheme (Fig. 6.7, 6.8) and was also compared with experiments. There is a mutual agreement.

Further we dealt with a numerical simulation of a turbulent compressible flow in the LONG for which we applied two turbulence models – an algebraic Baldwin-Lomax model (Fig. 6.9) and 2-equation $k-\omega$ model (Fig. 6.10).

The last test case was a 3D inviscid compressible flow around the SWEPT WING (Fig. 6.11) for which a **RK** scheme was used. Results were verified by **WLSQR** scheme (Fig. 6.12).

6. Conclusions. The work presents results of numerical methods solving 2D and 3D inviscid transonic flows using Lax-Wendroff and multistage Runge Kutta methods with applications in a 2D cascade compared to experimental results and 2D and 3D GAMM channel. Numerical results of 2D turbulent subsonic flows are compared using algebraic and $k-\omega$ turbulence model in the case of 2D cascade with separation domain near the trailing edge. All the methods were applied using our solver.

Acknowledgment. The work was partly supported by the Research Plan VZ MSM 6840770010 and by the grant projects GA AS CR IAA 2007 60 81, GA CR P101/10/1329 and SGS 10/243/OHK2/3T/12.

REFERENCES

[1] R. DVOŘÁK. *Transonic Flows*. Academia, Prague 1986 (in Czech).
[2] R. DVOŘÁK AND K. KOZEL. Mathematical modelling in aerodynamics, CTU in Prague, Prague 1996 (in Czech).
[3] A. FAVRE. *Équations des gaz turbulents compressibles*. Jour. de Mecanique **4** (1965), 361–390.
[4] M. FEISTAUER, J. FELCMAN AND I. STRAŠKRABA. *Mathematical and Computational Methods for Compressible Flow*. Oxford University Press, 2003.
[5] C. HIRSCH. *Numerical Computation of Internal and External Flows*. Volume II, - Computational Methods for Inviscid and Viscous Flows, John Willey&Sons, 1990.
[6] J. HOLMAN AND J. FŰRST. *Comparision of High Order Methods for Transonic Inviscid Flows*. Proceedings: Colloquium Fluid Dynamics 2008, 11-12, Institute of Thermomechanics, AS CR, v. v. i., Prague 2008.
[7] J. HUML, J. FŰRST, K. KOZEL AND J. PŘÍHODA. *Numerical Solution of Subsonic and Transonic Flows in a Channel*. Proceedings: Topical Problems of Fluid Dynamics 2009, 45-48, Institute of Thermodynamics, AS CR, v. v. i., Prague 2009 (in Czech).
[8] J. HUML, J. HOLMAN, J. FŰRST AND K. KOZEL. *Numerical Solution of 3D Inviscid Flows in a Channel*. Proceedings: Topical Problems of Fluid Dynamics 2010, 73-76, Institute of Thermomechanics, AS CR, v. v. i., Prague 2010.
[9] P. POŘÍZKOVÁ. *Numerical Solution of Compressible Flows Using Finite Volume Method*. PhD Dissertation CTU in Prague, Faculty of Mechanical Engineering, CTU in Prague, Prague 2009 (in Czech).
[10] J. PŘÍHODA AND P. LOUDA. *Mathematical modelling of turbulent flow*. CTU in Prague, Prague 2007 (in Czech).
[11] J. ŠIMONEK, K. KOZEL AND J. TREFILÍK. *Numerical Solution of Inviscid and Viscous Flows with Application*. Proceedings: Topical Problems of Fluid Mechanics 2007, 169-172, Institute of Thermomechanics, AS CR, v. v. i., Prague 2007.
[12] J. A. SETHIAN. *Level Set Methods*. Cambridge University Press (1996).

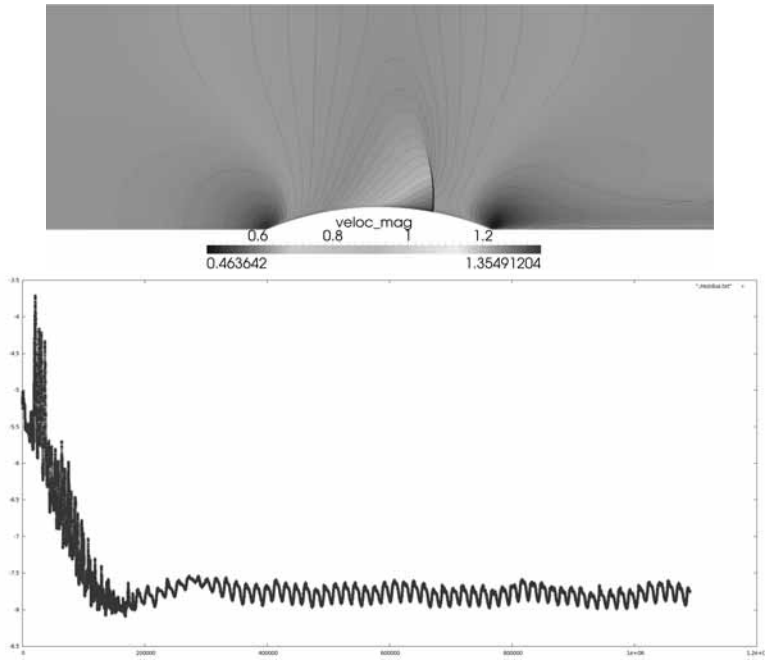

FIG. 6.1. *Inviscid compressible flow in the GAMM channel: Mach number isolines at* $M_1 = 0.675$ *(top) and* L_2 *logarithmic residuals (bottom) – MC scheme, IBC* $\mathcal{B}$ *[*$M_{max} = 1.35$*], a structured non-orthogonal grid with* 150×50 *cells.*

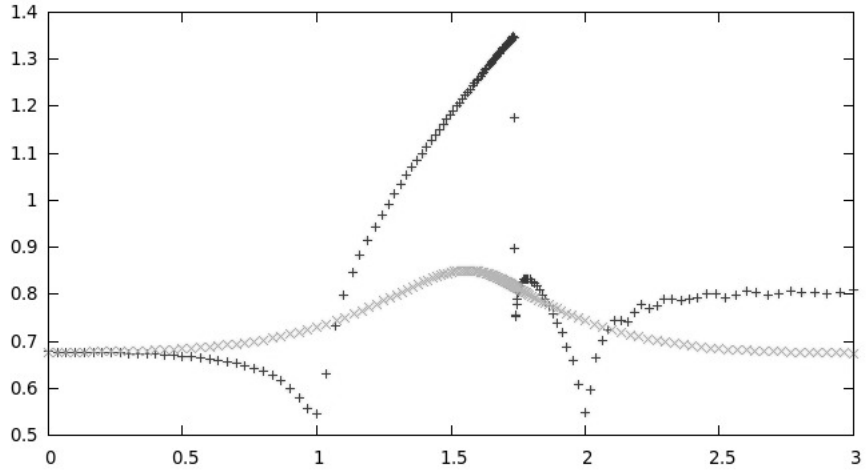

FIG. 6.2. *Inviscid compressible flow in the GAMM channel: distribution of Mach number on the lower wall at* $M_1 = 0.675$ *– MC scheme, IBC* $\mathcal{B}$ *[*$M_{max} = 1.35$*], a structured non-orthogonal grid with* 150×50 *cells.*

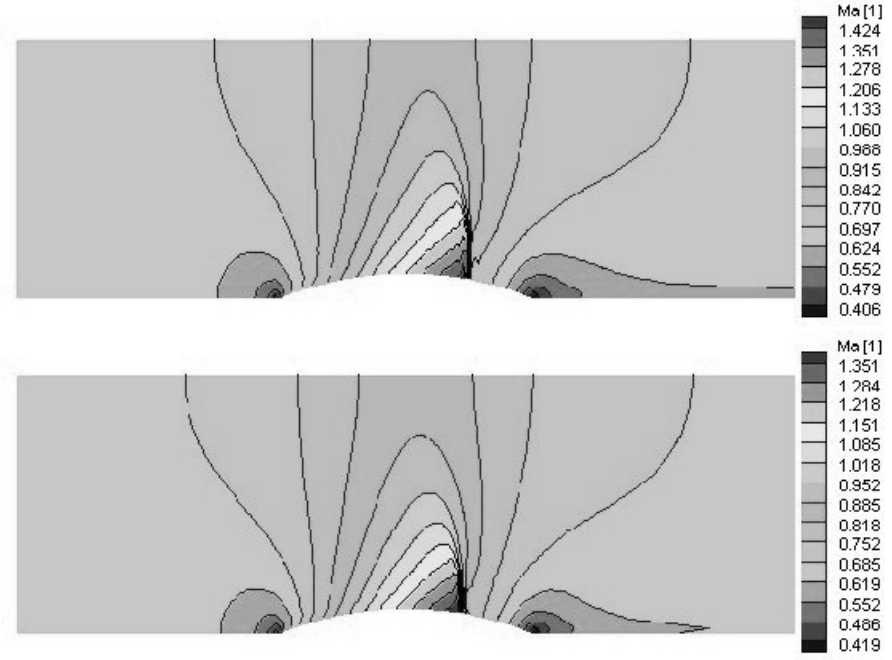

FIG. 6.3. *Inviscid compressible flow in the GAMM channel: Mach number isolines at* $M_1 = 0.675$ *– Ri scheme, IBC* $\mathcal{A}$ *[*$M_{max} = 1.42$ *(top)] and* $\mathcal{B}$ *[*$M_{max} = 1.35$ *(bottom)], a structured non-orthogonal grid with* 240×50 *cells.*

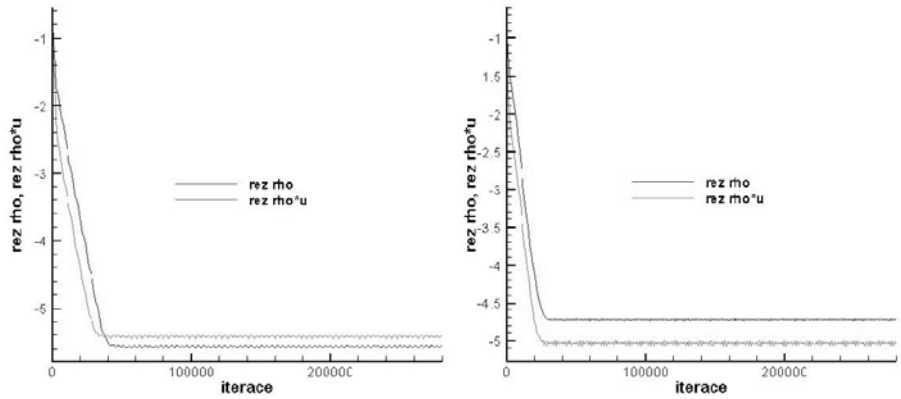

FIG. 6.4. *Inviscid compressible flow in the GAMM channel:* L_2 *logarithmic residuals at* $M_1 = 0.675$ *– Ri scheme, IBC* $\mathcal{A}$ *[*$M_{max} = 1.42$ *(left)] and* $\mathcal{B}$ *[*$M_{max} = 1.35$ *(right)], a structured non-orthogonal grid with* 240×50 *cells.*

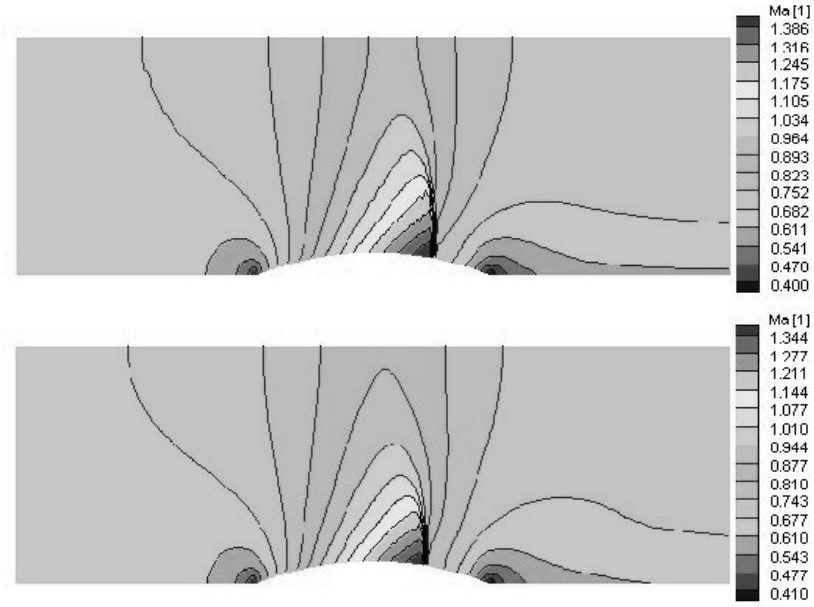

FIG. 6.5. *Inviscid compressible flow in the GAMM channel: Mach number isolines at* $M_1 = 0.675$ *– RK scheme, IBC* $\mathcal{A}$ *[*$M_{max} = 1.39$ *(top)] and* $\mathcal{B}$ *[*$M_{max} = 1.34$ *(bottom)], a structured non-orthogonal grid with* 240×50 *cells.*

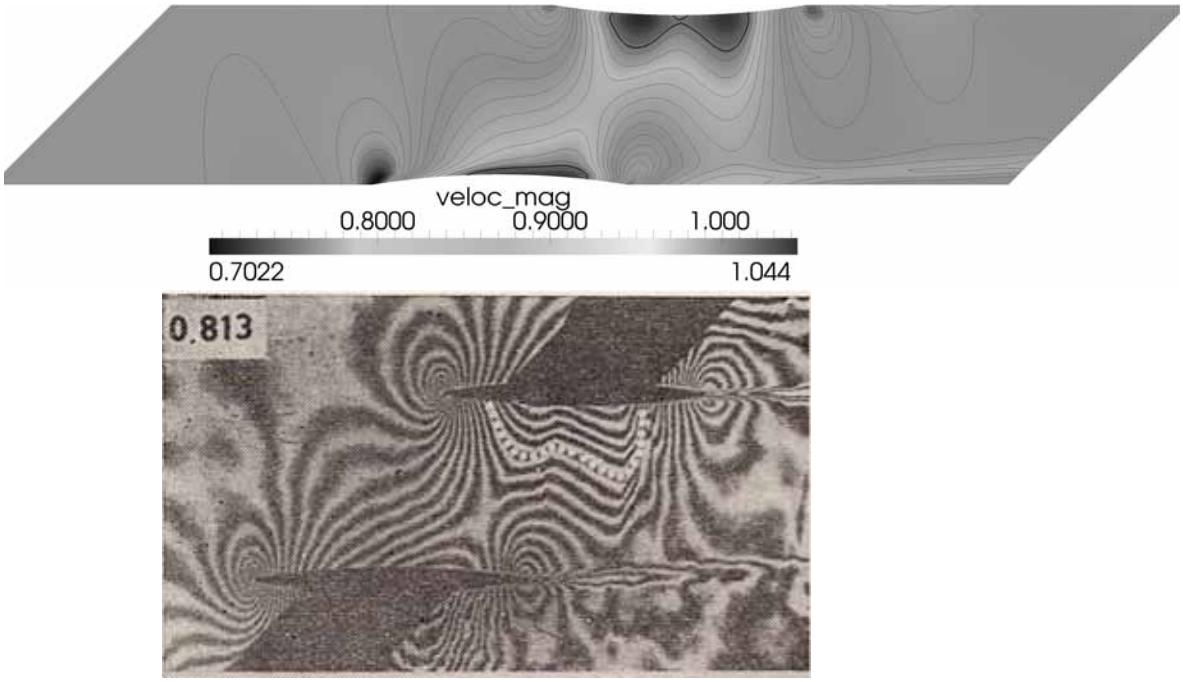

FIG. 6.6. *Inviscid compressible flow through the DCA 8% cascade: Mach number isolines at* $M_1 = 0.85$, $\alpha_1 = 0°$ *(top) and experiment by R.Dvorak [1] at* $M_1 = 0.813$ *(bottom) – MC scheme, IBC* $\mathcal{B}$*, a structured non-orthogonal grid with* 150×50 *cells .*

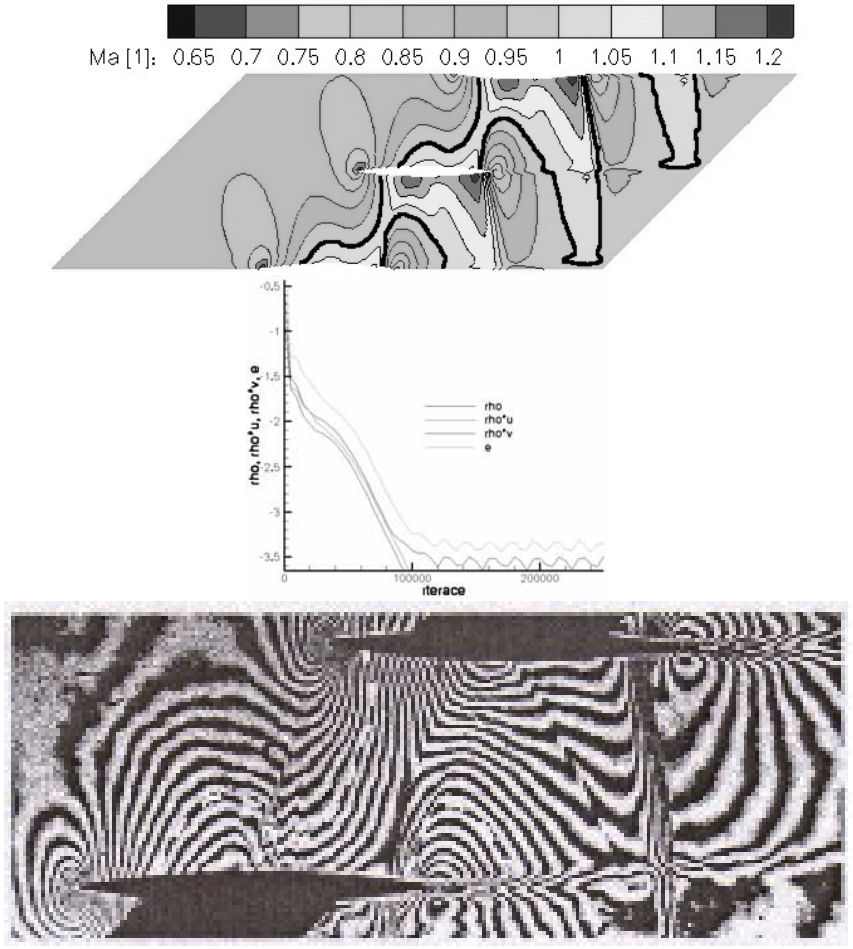

FIG. 6.7. *Inviscid compressible flow through the DCA 8% cascade: Mach number isolines at* $M_1 = 0.92$, $\alpha_1 = 2°$ *(first) and* L_2 *logarithmic residuals (second) – RK scheme, IBC* $\mathcal{A}$*, a structured non-orthogonal grid with* 140×50 *cells. Experiment by R. Dvorak [1] at* $M_1 = 0.863$ *(third)*

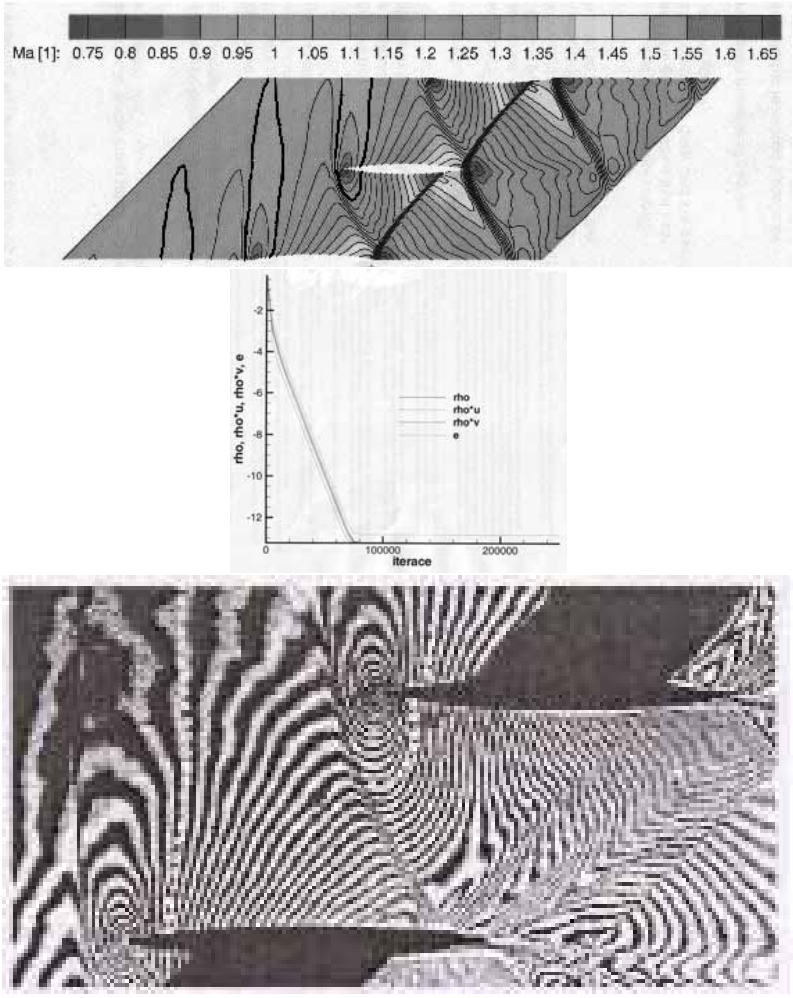

FIG. 6.8. *Inviscid compressible flow through the DCA 8% cascade: Mach number isolines at* $M_1 = 1.12$, $\alpha_1 = 0.5^\circ$ *(first) and* L_2 *logarithmic residuals (second) – RK scheme, IBC* $\mathcal{A}$*, a structured non-orthogonal grid with* 140×50 *cells. Experiment by R. Dvorak [1] at* $M_1 = 1.013$ *(third)*

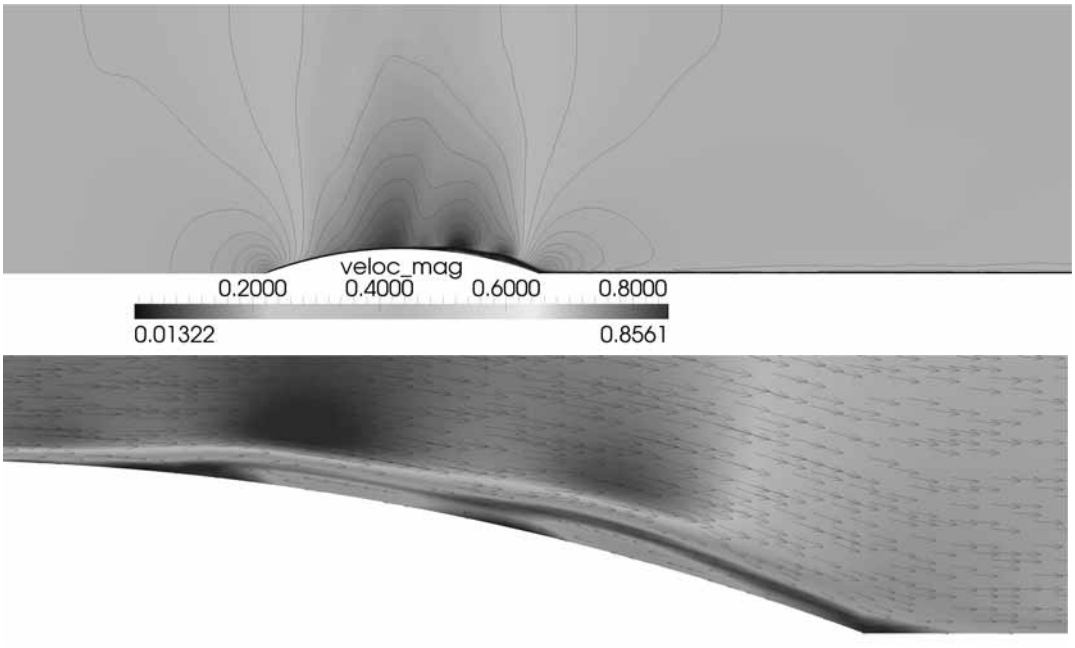

FIG. 6.9. *Turbulent compressible flow in the* LONG*: Mach number isolines at* $M_1 = 0.6$ *(top) and detail of separation near the end of the profile (bottom) – MC scheme, Baldwin-Lomax model, IBC* $\mathcal{B}$*, a structured non-orthogonal grid with* 150×30 *cells.*

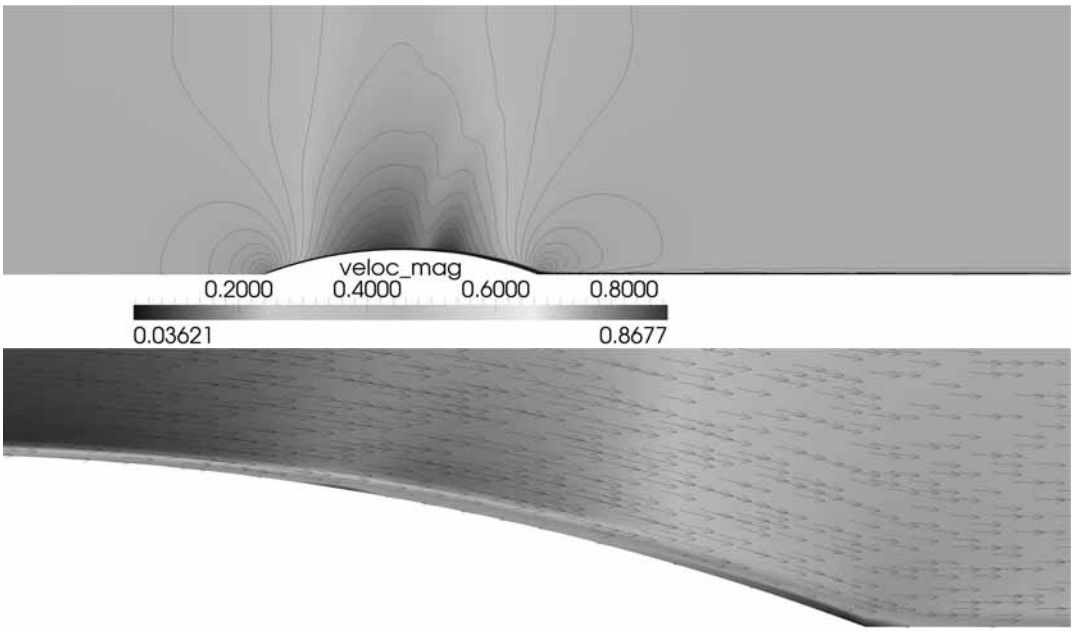

FIG. 6.10. *Turbulent compressible flow in the* LONG*: Mach number isolines at* $M_1 = 0.6$ *(top) and detail of separation near the end of the profile (bottom) – MC scheme,* $k - \omega$ *model, IBC* $\mathcal{B}$*, a structured non-orthogonal grid with* 150×30 *cells.*

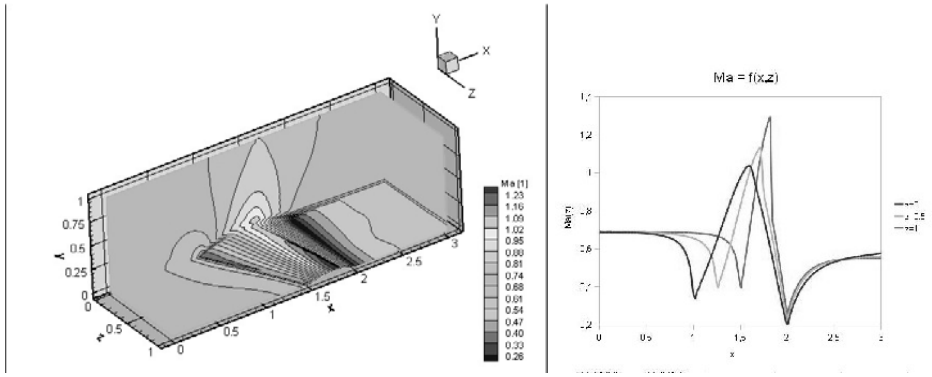

FIG. 6.11. *Inviscid compressible flow around the* SWEPT WING IN THE 3D GAMM CHANNEL*: Mach number isolines at* $M_1 = 0.675$ *(left) and distributions of Mach number on the lower wall in the slides (right) – RK scheme, IBC* $\mathcal{A}$*, a structured non-orthogonal grid with* $110 \times 30 \times 10$ *cells.*

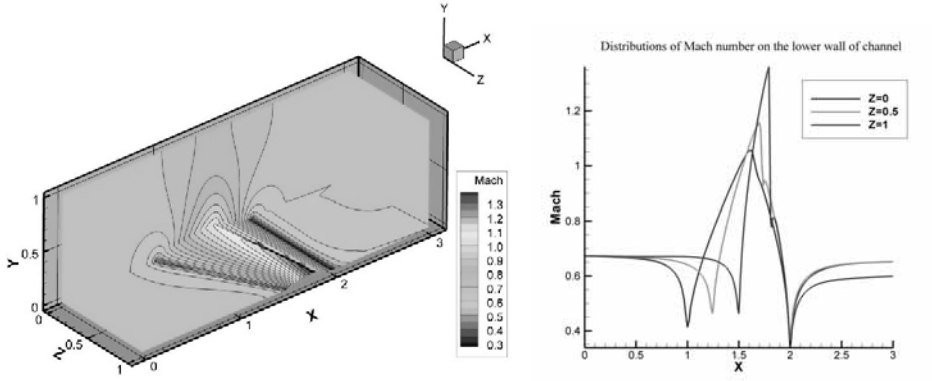

FIG. 6.12. *Inviscid compressible flow around the* SWEPT WING IN THE 3D GAMM CHANNEL*: Mach number isolines at* $M_1 = 0.675$ *(left) and distributions of Mach number on the lower wall in the slides (right) – WLSQR scheme by J. Holman [6], IBC* $\mathcal{A}$*, a structured non-orthogonal grid with* $180 \times 35 \times 35$ *cells.*